Computers in Industry 139 (2022) 103664

Contents lists available at ScienceDirect

Computers in Industry

journal homepage: www.elsevier.com/locate/compind

Structure-from-motion based image unwrapping and stitching for small bore pipe inspections

Dayi Zhang*, William Jackson, Gordon Dobie, Graeme West, Charles MacLeod

Centre for Ultrasonic Engineering, University of Strathclyde, 204 George Street, Glasgow G1 1XW, UK

ARTICLE INFO

Article history:
Received 25 October 2021
Received in revised form 22 February 2022
Accepted 22 March 2022
Available online xxxx

Keywords:
Small bore pipe inspection
Image processing
Visual inspection

ABSTRACT

Visual inspection is one of the most ubiquitous forms of non-destructive testing, being widely used in routine pipe inspections. For small bore pipes (centimetre diameter), inspectors often have a restricted field of view limiting overall image and inspection quality. Stitching multiple unwrapped images is a common inspection technique to provide a full view inspection image by combining multiple video frames together. A key challenge of this method is knowing the camera pose of each frame. Consequently, mechanical centralisers are often utilised to ensure the camera is located centrally. For the inspection of small-bore pipes, such mechanical centralisers are often too large to fit. This paper presents a post-processing, Structure-from-Motion (SfM) based approach to unwrap and stitch inspection images, captured by a manually deployed commercial videoscope. It advances state-of-the-art approaches which rely on the projection of a laser pattern into the field of view, thus reducing the equipment size. The process consists of camera pose estimation, preliminary point cloud generation, secondary fitting, images unwrapping and stitching to form an undistorted view of the pipe interior. Two industrial focussed demonstrators verified the successful implementation for small-bore pipe inspections. Whereby the new approach does not rely on image features to create the surface texture and is less sensitive to the image quality, more areas can be retrieved from inspections. The reconstructed area was increased by up to 87% using the new approach versus the conventional 3D model.

1. Introduction

1.1. Background

In the oil and gas industries, pipelines form a significant part of the essential infrastructure. Natural factors, which may include pressure, oxidation, and ageing materials, can cause critical damage to this infrastructure, reducing the safe working lifetime (Shukla and Karki, 2016).

Remote Visual Inspection (RVI) is a Non-Destructive Testing (NDT) method that uses a camera to evaluate the surface condition where the inspector operates the camera equipment remotely. Compared with some other NDT methods (such as ultrasound, eddy current), RVI has the benefits of compact size, provides flexibility to access confined spaces, e.g. small-bore oil and gas pipework (Reyes-Acosta et al., 2019). In addition, RVI requires minimal preparation of the pipework prior to inspection, and the inspection data is easily interpreted.

In the existing literature, RVIs are mainly conducted by handheld, pushrod cameras or visual inspection robots depending on the pipe internal bore diameter (Bibuli et al., 2007). Inspection robots are commonly used for the inspection of large inner diameter pipes (Eddyfi, 2020), while handheld rod and pushrod cameras offer access to smaller diameter pipes.

1.2. Inspection robots

Inspection robots, which may be utilised when the pipe diameter is significant enough to allow access are typically equipped with one or more cameras. Their enhanced payload allows for the inclusion of supplementary sensors to enhance the inspection. These robotic systems may also be remotely guided from one end to the other of the pipe for interior surface assessments allowing for navigation of complex systems which may not be possible with passive control. Further advantages of a robotic system is the capability for self-locomotion without requiring a tether or pushrod Hansen et al. (2015) leveraged this and developed a wireless system. Kawaguchi et al.

* Corresponding author.
E-mail address: dayi.zhang@strath.ac.uk (D. Zhang).

https://doi.org/10.1016/j.compind.2022.103664
0166-3615/

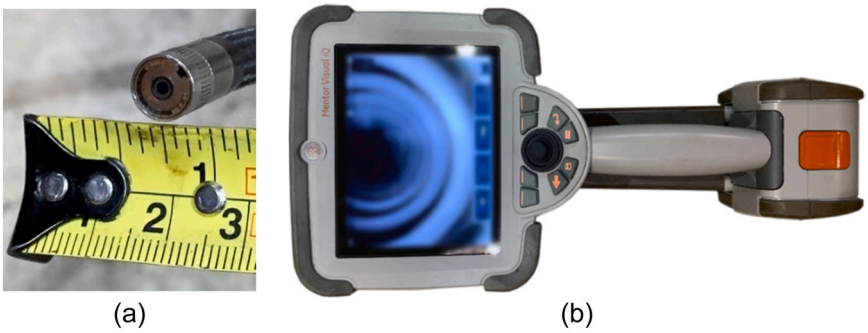

Fig. 1. (a) An inspection videoscope (header diameter 8.4 mm), with an embedded miniature camera. (b) The videoscope handheld, utilised to record inspection video footage.

(1995) prototyped an inspection crawler driven by a pair of magnetic wheels, providing capabilities to attach to internal surfaces of ferromagnetic pipes while undertaking visual inspections. Roh and Choi (2005) presented a spring-loaded mechanism to drive and steer within pipelines. Kwon and Yi (2012) utilised a similar spring-loaded mechanism to actively adapt to the pipe radius for camera centralisation. The robot also included an accelerometer, a gyroscope and wheel encoders to estimate the camera poses. Hansen et al. (2015) prototyped a crawler equipped with a fisheye camera and two laser diodes to inspect 400 mm diameter pipes. The system utilised structured-light techniques (Gang, 2011) to reconstruct a sub-millimetre accuracy 3D model of the pipe under inspection. J. Konig et al. equipped cameras and an inertial measurement unit on a hoisting cage to visually inspect a vertical mine shaft (König and O'Leary, 2020). Although robots have a precise degree of position control, the dimensions of such robots limit their abilities to be deployed in small bore pipes.

1.3. Handheld videoscope

Compared to a handheld device, inspection robots can deploy the camera with a far finer degree of position control and with greater repeatability. However, oil and gas pipes often have a small diameter (< 25 mm), which inspection robots are often too big to access and navigate which rules them out for inspection of such assets. Therefore, a more elegant solution is sought in the use of a handheld videoscope. A videoscope consists of an embedded miniature camera in the tip of the scope, as presented in Fig. 1. When using such videoscopes to conduct pipe inspections, the pipe length is limited by the maximum travel distance of the videoscope (up to 30 m) (Baker Hughes, 2020).

The scope is manually inserted into the pipe for inspections. Commercial miniature videoscopes offer the capability to inspect sub-millimetre diameter pipework (Baker Hughes, 2020; SPI Engineering, 2020). Kagami et al. (2020) utilised a videoscope to inspect and reconstruct pipe structures. In this work, the authors demonstrated the accuracy and robustness improvements with the introduction of cylindrical constraints. West et al. (2015) and Jackson et al. (2020) used such a camera to visually inspect pipe interior surfaces with mechanical centralisation methods to improve measurement accuracy. For the inspection of small-bore pipes, such mechanical centralisers are often too large to fit within the bore or navigate bends.

1.4. RVI approaches

Conventional RVI approaches are utilised to evaluate surface conditions and result in decisions of the condition of the asset from recorded or live images of the pipework under inspection (Sergiyenko et al., 2020). Such approaches are typically regarded as qualitative analysis due to the lack of conveying position and location information of detected defects. Despite many inspection robots being equipped with motion sensors (such as encoders) to estimate insertion distance (Kwon and Yi, 2012; Zhang, 2022; Eddyfi, 2020), the location estimations are often inaccurate due to the accumulating error with insertion distance. The distance is generally measured from these sensors which are known to suffer from slippage leading to the aforementioned error.

Creating textured 3D photogrammetric models is one of the post-processing techniques utilised in visual inspections. After the inspection, a textured 3D model is reconstructed to provide a more contextual assessment of the target object. Reconstruction is the process of generating a computer model of the 3D profile of an object from a set of 2D images. Therefore, the resulting 3D model implicitly displays surface feature locations. By estimating the approximate location of each image, reconstruction represents a feasible approach to localise the defects on the pipe under inspection. Implementations of such a method include the inspection of mining shafts (König and O'Leary, 2020) but also for pipes (Zhang et al., 2019; Kagami et al., 2020). Textured 3D reconstruction modelling is based on Structure from Motion (SfM) (Snavely et al., 2006). The technique of SfM (Snavely et al., 2006) involves extracting the unique features from a collection of 2D images and matching these features to estimate sparse scene geometry and camera positions. The sparse point cloud and estimated camera positions generated by SfM are further processed by application of Multiview Stereo algorithms (Furukawa and Ponce, 2010), which calculate densified point clouds to render an accurate 3D geometry. The accuracy of the reconstructed 3D model is highly dependent on the quality of the images. Low light intensity can reduce the image quality, leading to the reduction of the number of features on captured images which is a critical factor in the 3D reconstruction process (Bianco et al., 2018; Zhang et al., 2020). Although videoscopes and inspection robots are often equipped with LEDs for illumination, the LEDs cannot always cover all areas within the camera's field of view. This is a particular problem when using un-centralised videoscopes, as the LEDs tend to be forward facing mounted in a ring around the lens, when unaligned with the pipe axes there are often areas of significant over exposure and underexposure. Thus, areas of the image remain which have imperfect brightness to acquire surface features and therefore introduce errors during reconstruction and texture rendering.

Panorama imaging is another visualisation method which presents inspection results as a single high-resolution image with an elongated field of view. It is built from stitching multiple images captured in different poses with the use of computer vision algorithms, such as SIFT feature matching (Brown and Lowe, 2007; Zhang et al., 2016). Therefore, it provides a more contextual assessment of the pipe interior condition. Compared with traditional RVI inspections composed of isolated video frames, the panorama image extends the field of view and provides results with intrinsic position and dimension information that are of great utility in the production of meaningful surface condition evaluations. Such a

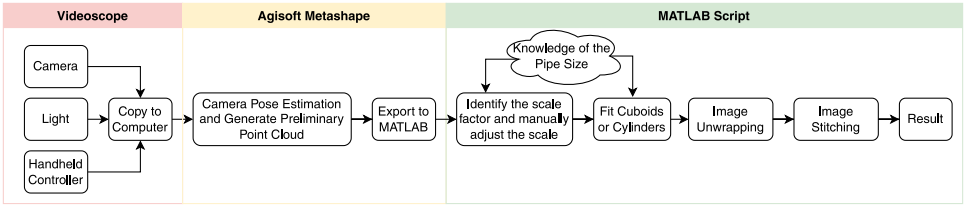

Fig. 2. Flow chart of the overall process.

technique has been featured in the literature on vision inspections (Xie et al., 2018; König and O'Leary, 2020). Before being stitched into a panorama image for internal surface inspections, the raw images must be unwrapped and projected onto a flat plane. Conventionally, the probe would be deployed with a mechanical centraliser to maintain the camera at the centre of the pipe, so that the image unwrapping can be directly approached by using a transform function based on the camera and lens parameters (West et al., 2015; Jackson et al., 2020). However, due to the limited access, such mechanical centralisers are not practical for small-bore pipe inspections. Using a laser projector is another possible approach, which recovers the camera pose by projecting a laser ring onto the pipe surface. The reflections with distorted patterns are captured by the camera to estimate the camera pose. Duran et al. (2007) utilised the laser profile, projected on the pipe to estimate the camera poses. The images can be centralised during the post-processing using calculated camera poses. Hosseinzadeh et al. (2021) demonstrated the accuracy of such methods was a 90% confidence interval of ± 0.5 mm and ± 0.5° in translation and rotation changes.

2. Aim and objectives

The literature demonstrates various approaches for internal pipe inspections. These approaches are generally designed for large-bore pipes, which allows for the use of additional hardware to centralise the videoscope or estimate the camera poses. Thus, the aim is to create a novel approach to use un-centralised commercial videoscope without external hardware for small-bore pipe inspections.

Because of the access limitation of small-bore pipes (diameter < 25 mm), a thin videoscope (Baker Hughes, 2020) without extra hardware (e.g. centraliser (Jackson et al., 2020), laser projector (Duran et al., 2007) is used in this paper (as shown in Fig. 1). The videoscope is outfitted with an LED array which provides illumination of the internal surface of the pipework.

The accuracy of the 3D reconstructed model depends on the image quality. Image features are the key factors in the 3D reconstruction process (Snavely et al., 2006). This is problematic due to the nature of the low illumination inside pipework and un-centralised camera poses. Images captured under such an environment lack the detailed features of the pipe surface. This leads to the failure of the texture extraction process and hinders the 3D reconstruction. The panoramic images built by the authors' synthetic approach will mitigate such impacts and maintain inspection accuracy.

Fig. 2 presents a flow chart of the inspection approach. The inspector inserts the handheld videoscope through a small-bore pipe, gathering the required image frames. Then, inspection data are transferred to the computer for further post-processing. The camera poses and the point cloud of the pipework are preliminary reconstructed using conventional SfM through the commercial software package Agisoft Metashape (Agisoft LLC, 2020). The point cloud post-processing and the secondary point cloud fitting are implemented in MATLAB (MathWorks, 2021). After point cloud fitting, a MATLAB script unwraps the images and stitches them together to create high-quality stitched image panoramas which is the ultimate aim of this work.

The remainder of the paper is structured as follows, Section 3 presents the methodology for camera pose and point cloud generation. Sections 4 and 5 present the image unwrapping and stitching respectively. Section 6 demonstrates the practical inspection results using the approach presented in this paper. Finally, in Section 7, the paper is concluded with a discussion of results.

The main contributions of this paper are:

- Develop an approach for creating high-quality unwrapped and stitched image from un-centralised videoscope small-bore pipe inspections. The approach uses commercial SfM software to estimate the camera poses and generate a preliminary point cloud. From this a stitched image to extend the field of view is created. Because of the knowledge of target inspections (shape and diameter), the process is simplified and more robust.
- Unwrapped frames are created from footage captured by existing commercial videoscopes without extra hardware. Thus, it reduced the size of the tool and broadened its applicability to include sub-millimetre diameter pipework.
- The approach is demonstrated on practical oil and gas pipe inspections.
- Due to the lack of unique features, some surface areas may be missing in the 3D model. This approach successfully recovered these surface areas on the panoramas.

3. Point cloud generation

In this study, the camera pose estimation and the preliminary point cloud generation were conducted via Agisoft Metashape (Agisoft LLC, 2020), a commercial software package which performs photogrammetric processing of discrete images and generates 3D spatial data. The main technique used in this software is SfM, which assumes the images are captured from a single camera in a series of unknown camera locations and orientations. It estimates the camera poses by extracting and matching the unique features from consecutive images. The camera is calibrated using the MATLAB camera calibration toolbox (MathWorks, 2020) and optimised by Agisoft's proprietary algorithms (Agisoft LLC, 2020) during the reconstruction process. Point cloud, mesh and textured models are built in sequence after camera poses estimation to create a detailed 3D profile. It is worth noting that due to the dimensionless nature of the photogrammetry technique, the scale is unknown during the reconstruction process and, as such, the software output does not contain the absolute sizing of the model (Agisoft LLC, 2020). Therefore, a scaling factor relating to the camera poses and 3D profile is calculated by dividing the pipe's known ground truth diameter by the 3D profile diameter.

Fig. 3 shows a point cloud of a segment of 20 mm width and height box section and the camera poses during the experiment. These are generated by Agisoft Metashape. The colour map represents the point cloud density, given by the number of points within a volume of size 1 mm^3. Lower density areas occur due to less features having been extracted from the raw images used to reconstruct the region, reduced features in specific regions within a uniform sample largely arise due to motion blur or low light

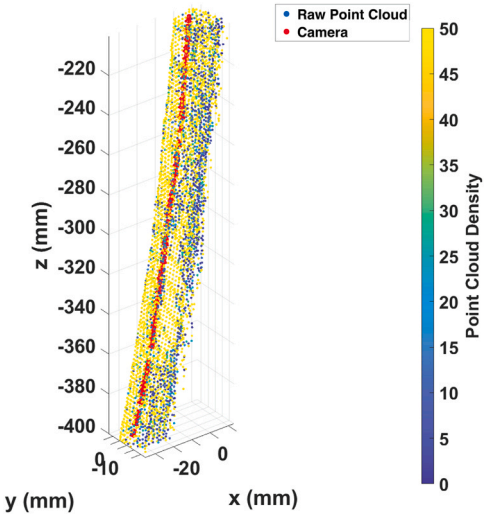

Fig. 3. An example of the point cloud and the camera poses calculated by the Agisoft Metashape.

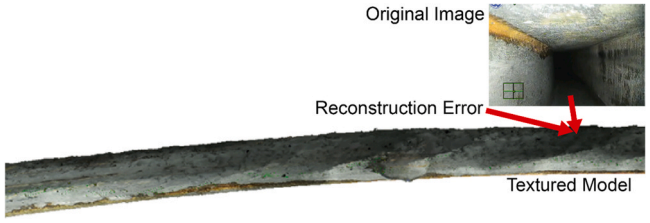

Fig. 4. An example of the textured model reconstructed by the Agisoft Metashape. The bottom regions were not fully covered by the LEDs, causing errors on the texture model.

intensity. Fig. 4 presents the textured model of the same box section under inspection.

As shown in Fig. 3, the point cloud contains many outliers and considerable noise, which can also be identified as discontinuities on the textured reconstruction (Fig. 4). Such discontinuities and outliers are artificial errors added during the reconstruction process. As presented in Fig. 12, these errors can hide and distort real surface detects, causing inspector misjudgements and potential risks of structural failures. As shown in Fig. 4, the errors during the reconstruction process are often in regions that were not covered by the onboard LEDs during the inspection. The images captured under imperfect illumination lack detailed features of the pipe surface, leading to Metashape being unable to accurately extract and match the pipe details in these regions. Defects and discontinuities in these unilluminated regions are hidden in the textured model, leading to the consequential inability of using the reconstructions for an accurate and complete inspection.

Metashape generates the point cloud and mesh without any prior knowledge of this model. Kagami et al. (2020) demonstrated significant improvements after applying constraints during the SfM process. The prior cylinder constraints assume the model shape is cylindrical and refine the SfM optimisation results to be a more specific cylinder model. However, it is impractical to implement such constraints within a commercial software package such as Metashape. Therefore, a secondary point cloud fitting is implemented to create a structure using characteristics extracted from the preliminary point cloud. These characteristics, including the pipe geometry and orientation are automatically extracted by a custom MATLAB script. The geometry of the secondary fitting depends on the actual pipe structure. Cuboids are utilised for rectangular box sections (as shown in Fig. 5), and cylinders are for round pipes (as

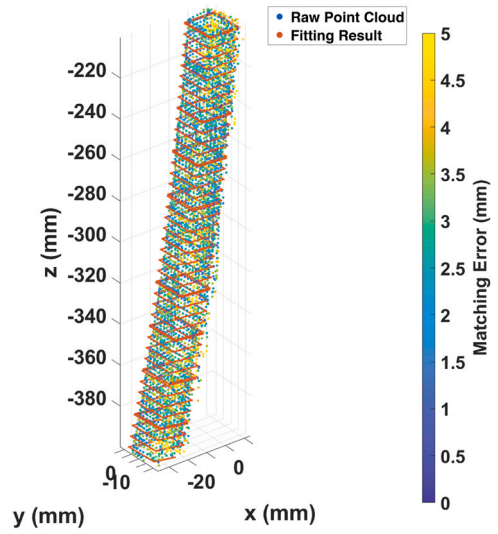

Fig. 5. Point cloud of a part of box section reconstructed by the Agisoft Metashape and the fitted cuboid.

presented in Section 6.1). The geometry of the cuboids (height and width) and the geometry of the cylinder (diameter) are defined by the known size of the pipe under inspection.

To cover pipe bends, the point cloud is sliced into multiple sections, each with a length equal to the pipe diameter and fitted individually. The fitting procedure adjusts the poses of the fitted pipe sections to minimise the average of the Euclidean distance between the structure (cuboid or cylinder) and Metashape point cloud. Compared with the point clouds generated by Metashape, the fitting process reduced the noise and estimated the geometries of the regions which are not generated by the software. Therefore, the Metashape point cloud is replaced by the fitted structure in the remaining processing steps. Fig. 5 depicts a section of the rectangular pipe's point cloud from Metashape and its fitting results using a cuboid structure.

As shown in Fig. 5, the regions observed to have low density (Fig. 2) also have relatively higher matching errors, demonstrating the profound impact of image blur and light intensity on the accuracy of the SfM-reconstructed model.

4. Image unwrapping

Image unwrapping is the projection of the points from the 3D coordinate frame onto a 2D image plane, which unwraps the internal pipe surface onto an image. Depth-Image-Based-Rendering (DIBR) (Fehn and Hhi, 2004) is utilised in the method which is outlined as follows and shown graphically in Fig. 6.

Firstly, a blank 2D image (Fig. 6(a)) is created. The height of the unwrapped image depends on the camera focal range and light coverage. The bottom of the image is the cross-section of the pipe at the camera position. The top of the image is 100 mm in front of the camera, beyond this point the original image from the videoscope becomes blurred and insufficiently illuminated. The 2D array has a ratio between X and Y in pixels as the circumference to height of the pipe section to ensure the unwrapped image is correctly scaled.

Secondly, as shown in Fig. 6(b), for each pixel in the 2D image, the pixel is mapped onto a cylinder or cuboid with the radius/width and axis angle as determined in Section 3.

Then, these points, now in the world coordinate (X, Y, Z) are projected to the camera coordinates (u,v) using the camera projection (Fig. 6(c)).

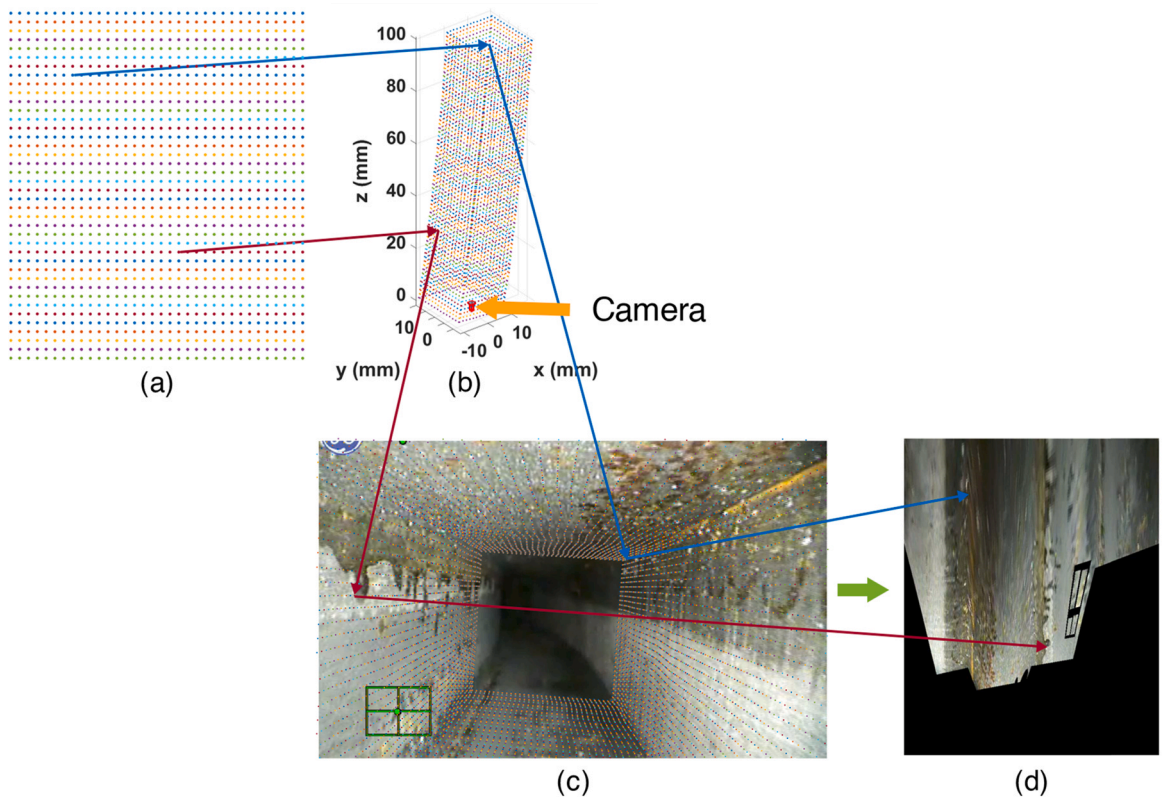

Fig. 6. The image unwrapping process. The blue and red lines represent corelations between the unwrapped image, the original image, and the fitted pipe. (a) the blank 2D image. (b) the image mapped onto the fitted pipe (c) the points projected on the original image (d) the unwrapped image with colour. The black section of the image shows sections which are not presented in the camera's field of view.

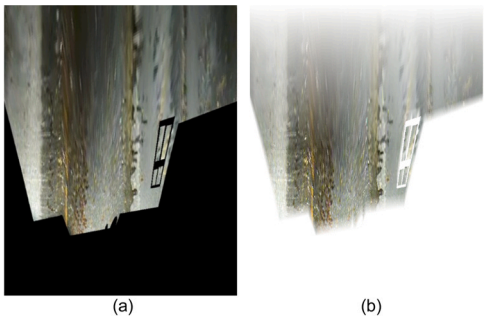

Fig. 7. The inspection image of a rectangular pipe under the inspection (a) the raw unwrapped image (b) the unwrapped image with the weight factor (transparent layer).

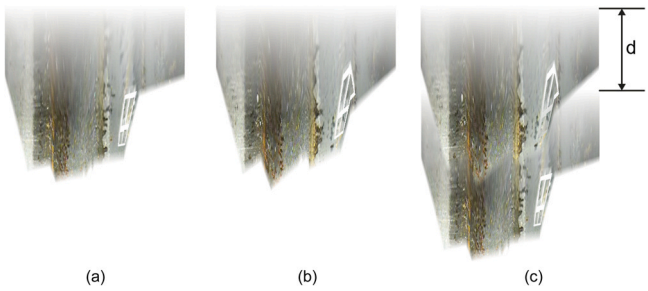

Fig. 8. The process of the image stitching. (a) and (b) are the unwrapped images to be stitched. The distance between (a) and (b) is calculated by the Metashape during the camera pose estimation. Move down (a) by the distance d and append (b) to get (c).

Finally, the colour information at the point (u,v) on the original camera image is applied to the 2D image generated at the first step of the process (Fig. 6(d)).

The camera projection model utilised in the paper is (Agisoft LLC, 2020):

$$x = \frac{X}{Z}, \quad y = \frac{Y}{Z} \tag{1}$$

$$u = x f_x + c_x, \quad v = y f_y + c_y \tag{2}$$

Where X, Y and Z are the point position in the world coordinate. u and v are the point position in the camera coordinate (in pixels). f_x and f_y are the focal lengths along the x and y axis. c_x and c_y are the principal point offsets along the x and y axis. These parameters are obtained during the camera calibration and optimisation process. Note that the camera's radial and tangential distortions are neglected because the values obtained during the calibration were small enough to have no significant effect, and the camera distortions are calibrated prior to inspection (Baker Hughes, 2020).

4.1. Panorama image stitching

Due to the nature of the low light intensity inside the pipe and the limited camera working distance, the unwrapped image contains many blurred features. Mixing these featureless parts with sharper and more detailed regions will reduce the quality of the result images. Thus, a weight factor is assigned to every pixel on each image to reduce the contributions of these unfocused pixels in the stitched images. In this paper, the pixels in the centre of the image have the maximum contribution (1), while the pixels at the edges have the lowest contribution (0). The contribution is linearly increased from the edge until it reaches the maximum. Fig. 7 is an

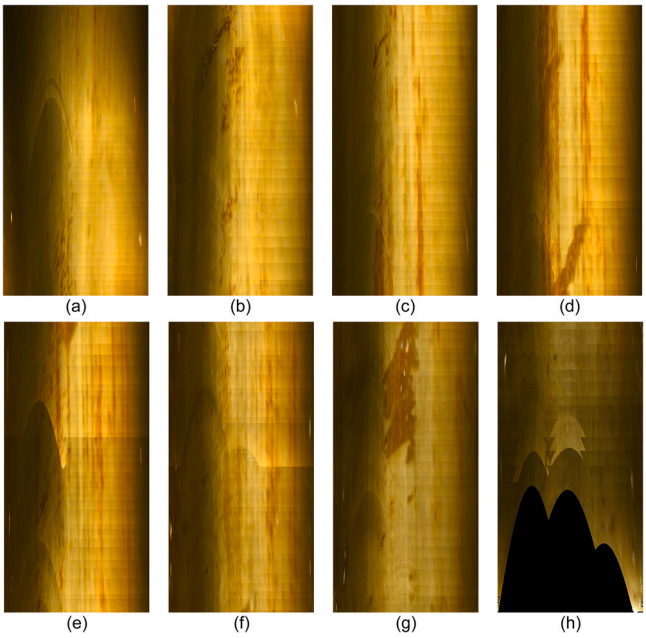

Fig. 9. The stitched panorama image of the copper pipe. As shown in (a) – (f), the camera was tilted towards bottom side of the pipe. The light intensity on the bottom side is much higher than the other side. The camera in (g) and (h) was moved back to the central, which produced a relatively better light distribution.

example of the blending contribution. Note that the pixel contribution is defined in the image's transparency layer. Greater transparency represents a lower contribution.

These unwrapped and weighted images are then stitched together to create a panorama image, as shown in Fig. 8. The pixels are averaged from the related images with the calculated weight factors. As the images have been aligned to be parallel to the pipe axis during the unwrapping process, the only variable required for the image stitching is the distance d between each image (as presented in Fig. 8(c)), which is obtained from the Metashape estimated camera poses. Because the unwrapped images and the stitched images are of the same scale factor, defect locations in world coordinates are linearly correlated to pixel positions on the stitched image allowing for localisation from the panorama.

4.2. Experiment results

The approach was verified by conducting two sets of empirical experiments. The first image set is from an inspection of a retired 15 mm diameter straight exchanger pipe. The second inspection is of an in-service 20 mm, curved rectangular oil pipe. Both pipes were manually inspected by an inspector using a videoscope (Baker Hughes, 2020), and following a standard procedure (British Standards Institution, 2016). The inspector conducted two standard visual inspections which moved the videoscope through the pipe with un-centralised camera poses. These poses caused significant variation in light intensity on the images, which presents considerable challenges during the 3D reconstruction which our method aims to overcome. As well utilised pipes, their internal surfaces contain many areas of corrosions and several detects, which are representative of typical industrial assets.

4.3. Exchanger pipe

The videoscope was manually deployed inside the pipe and covered an axial distance of 754 mm. Fig. 9 presents the sections of the stitched panorama image. Fig. 10 shows the Metashape reconstructed mesh using the same dataset.

Although Metashape successfully estimated the camera poses, as shown in Fig. 10, it failed to reconstruct a sufficiently complete 3D model of the exchanger pipe. This is because the camera was not centralised within the pipe, leading to a lack of illumination on one side, resulting in insufficient unique surface features for the 3D reconstruction. In contrast, as shown in Fig. 9, the panorama image utilising the secondary fitting and unwrapping strategy successfully reconstructed the missing side of the 3D model. Detailed surface features such as internal corrosion of the pipe is visible in the panorama images. The surface area of the stitched panorama image is 35,438 mm^2, increased by 87% from the Metashape reconstructed area (18,946 mm^2). The time taken to post-process the dataset was 10 min using a single thread on a desktop CPU.

4.4. In-service rectangular pipe

Similar to the copper pipe inspection, the videoscope was manually inserted a distance of 1834 mm into the rectangular pipe. Fig. 11 and Fig. 12 show the stitched panorama image and the comparisons to the Metashape reconstructed mesh, respectively.

Compared with the clean surfaces of the copper exchanger pipe, there were remnants of oil and other build ups of material within the rectangular pipe, these presented themselves as obstacles during the inspection. Such obstacles may cover the camera lens and potentially damage the videoscope. Thus, the camera was manoeuvred to avoid such obstacles during the inspections. The manoeuvres drifted the camera significantly close to the pipe surface, causing significant variation in illumination, areas which were underexposed had increased amounts of noise and artefacts within the reconstructed mesh. In contrast, as shown in Fig. 12, the textures on the panorama image in these areas are sharper, and defects can still be identified which was not possible directly from the textured model. The textured model includes more distorted features due to the source images containing degradations caused by the insufficient illumination and focal blur, as shown in Fig. 12(a)(c)(e). Fig. 12(b)(d)(f) displays the textures of the panorama image. Notably, as presented in Fig. 10(f), some areas of corrosion were observable on the panorama image, while these are hard to identify from the textured model. Because the images contained more distinctive textures than sample used in Section 6.1, the Metashape and panorama image are both deemed to have successfully reconstructed the pipe. The reconstructed area of the panorama image was just 5% greater in terms of surface area when compared with the Metashape mesh, from 138,973 mm^2 to 146,960 mm^2. The post-processing of this dataset took 38 min using the same hardware as Section 6.1.

Fig. 10. Metashape reconstructed 3D model. As shown in the figure, the software failed to reconstruct a complete 3D model.

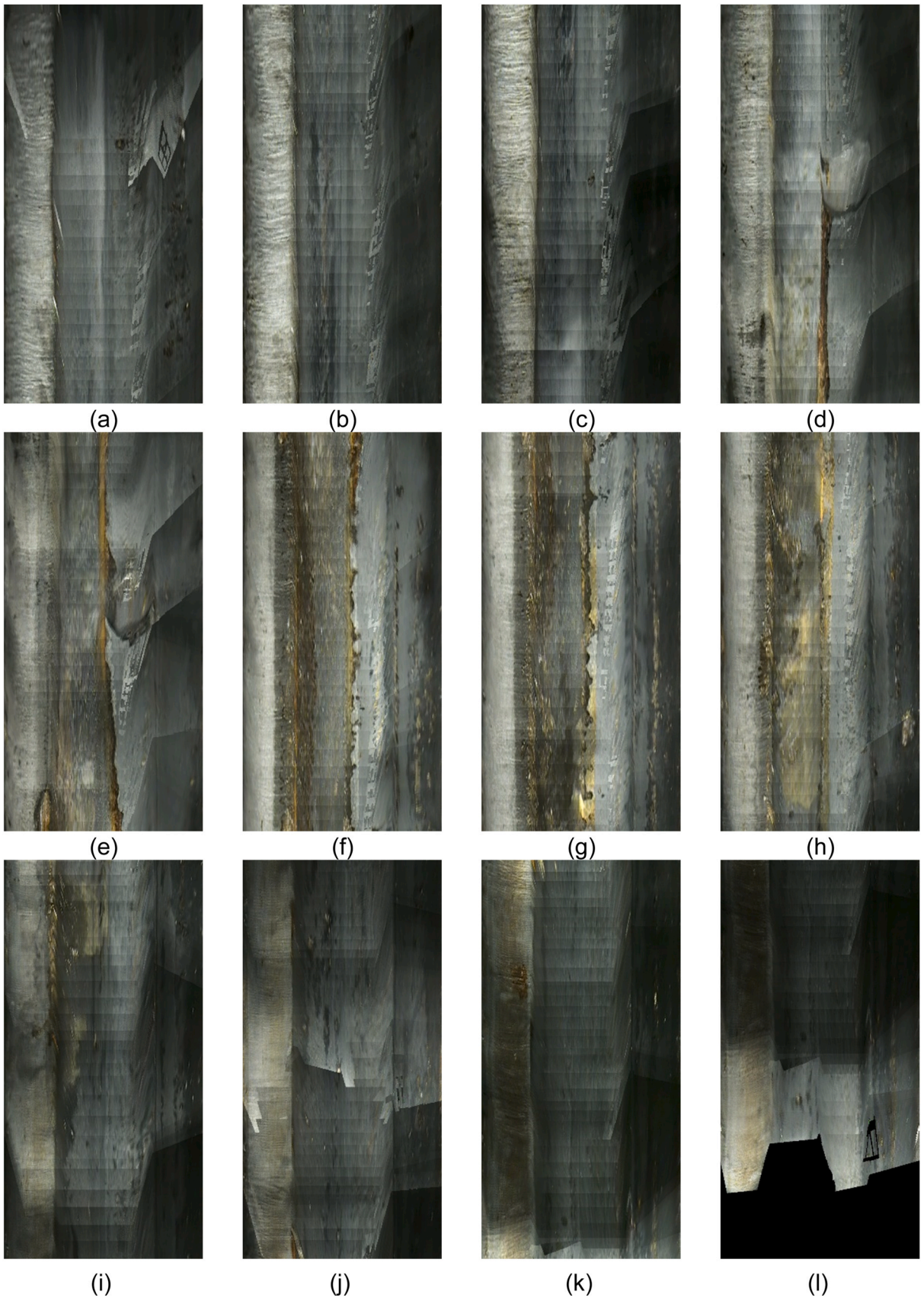

Fig. 11. The stitched panorama image of the rectangular pipe.

Fig. 12. The texture comparisons between the textured mesh (a)(c)(e) and the panorama image of the rectangular pipe (b)(d)(f).

5. Conclusion

This paper presents a novel visual inspection method, combining SfM algorithms, image unwrapping and stitching to inspect small-bore pipes. SfM was utilised to estimate the camera poses and generate point clouds, while the image unwrapping and stitching offered a stitched panorama image to extend the field of view. A secondary fitting was utilised to improve the point cloud quality greatly via imposing extra constraints. Compared to the state-of-the-art strategies, the new approach offers access to small-bore pipes using existing commercialised videoscopes without additional hardware. Thus, it reduced the size of existing tools required for such an inspection and broadened its applicability to include sub-millimetre diameter pipework with videoscopes sized appropriately. Additionally, the approach reconstructed the texture of regions captured with low light intensity, whereas the textures are blurry or absent using state-of-art SfM approaches. Consequently, significant area increases (by up to 87%) were observable in the inspection panorama images. The results of the two practical pipe inspections demonstrated the effectiveness of the panorama images produced with the presented approach. These results show a novel method and avenue to improved outcomes for remote vision inspections of oil and gas pipes in the field. Note that the post-processing in this paper is purely loaded on a single CPU thread. The MATLAB script has not been fully optimised for time efficiency and does not include any hardware acceleration. Future work will consider optimisations to reduce time consumption.

Funding

This work was supported in part by the Oil and Gas Innovation Centre (OGIC) in collaboration with Inspectahire Ltd (Aberdeen, UK).

CRediT authorship contribution statement

Dayi Zhang: Undertaking experiments, Writing. **William Jackson**: Writing. **Gordon Dobie, Graeme West, Charles MacLeod**: Writing – review & editing, Supervision.

Declaration of Competing Interest

The authors declare that they have no known competing financial interests or personal relationships that could have appeared to influence the work reported in this paper.

References

Zhang, D., et al., 2022. A framework of using customized LIDAR to localize robot for nuclear reactor inspections. IEEE Sens. J. 22 (6), 5352–5359. https://doi.org/10.1109/JSEN.2021.3083478

Agisoft LLC (2020) Agisoft Metashape User Manual: Professional Edition, Version 1.6. Available at: ⟨https://www.agisoft.com/pdf/metashape-pro_1_6_en.pdf⟩ (Accessed: 1 October 2020).

Baker Hughes (2020) Baker Hughes Video Borescopes. Available at: ⟨https://www.bakerhughesds.com/inspection-ndt/remote-visual-inspection/video-borescopes⟩ (Accessed: 21 July 2020).

Bianco, S., Ciocca, G., Marelli, D., 2018. Evaluating the performance of structure from motion pipelines. J. Imaging 4 (8). https://doi.org/10.3390/jimaging4080098

Bibuli, M., Caccia, M. and Lapierre, L. (2007) 'Robotic Devices for Water Main In-Pipe Inspection: A Survey', IFAC Proceedings Volumes (IFAC-PapersOnline), 7(PART 1), pp. 81–86. doi: 10.1002/rob.

British Standards Institution (2016) 'Bs En 13018:2016'.

Brown, M., Lowe, D.G., 2007. Automatic panoramic image stitching using invariant features. Int. J. Comput. Vis. 74 (1), 59–73. https://doi.org/10.1007/s11263-006-0002-3

Duran, O., Althoefer, K., Seneviratne, L.D., 2007. Automated pipe defect detection and categorization using caniera/laser-based profiler and artificial neural network. IEEE Trans. Autom. Sci. Eng. 4 (1), 118–126. https://doi.org/10.1109/TASE.2006.873225

Eddyfi (2020) Versatrax 150 Pipe Inspection Crawler. Available at: ⟨https://eddyfi.com/en/product/versatrax-150-pipe-inspection-crawler⟩ (Accessed: 21 July 2020).

Fehn, C., Hhi, H., 2004. Depth-image-based rendering (DIBR), compression and transmission for a new approach on 3D-TV'. Proc. SPIE 5291, 93–104.

Furukawa, Y., Ponce, J., 2010. Accurate, dense, and robust multiview stereopsis. IEEE Trans. Pattern Anal. Mach. Intell. 32 (8), 1362–1376. https://doi.org/10.1109/TPAMI.2009.161

Gang, J., 2011. Structured-light 3D surface imaging: a tutorial. Adv. Opt. Photonics 3, 128–160. https://doi.org/10.1364/AOP.3.000128

Hansen, P., et al., 2015. Visual mapping for natural gas pipe inspection. Int. J. Robot. Res. 34 (4–5), 532–538. https://doi.org/10.1177/0278364914550133

Hosseinzadeh, S., et al., 2021. A novel centralization method for pipe image stitching. IEEE Sens. J. 21 (10), 11889–11898. https://doi.org/10.1109/JSEN.2020.3031637

Jackson, W., et al., 2020. Error analysis and calibration for a novel pipe profiling tool. IEEE Sens. J. 20 (7), 3545–3555. https://doi.org/10.1109/JSEN.2019.2960939

Kagami, S., et al., 2020. 3D pipe network reconstruction based on structure from motion with incremental conic shape detection and cylindrical constraint. 2020-June. IEEE Int. Symp. . Ind. Electron. 1345–1352. https://doi.org/10.1109/ISIE45063.2020.9152377

Kawaguchi, Y. et al. (1995) 'Internal pipe inspection robot', Proceedings - IEEE International Conference on Robotics and Automation, 1, pp. 857–862. doi: ⟨10.1109/robot.1995.525390⟩.

König, J., O'Leary, P., 2020. Hyper resolution image mosaics with unbounded vertical field of view. Comput. Ind. 122. https://doi.org/10.1016/j.compind.2020.103281

Kwon, Y.S., Yi, B.J., 2012. Design and motion planning of a two-module collaborative indoor pipeline inspection robot. IEEE Trans. Robot. 28 (3), 681–696. https://doi.org/10.1109/TRO.2012.2183049

MathWorks (2020) Camera Calibration and 3-D Vision. Available at: ⟨https://uk.mathworks.com/help/vision/camera-calibration-and-3-d-vision.html⟩.

MathWorks (2021) *MATLAB*, Online Webpage. Available at: ⟨https://uk.mathworks.com/products/matlab.html⟩ (Accessed: 1 January 2022).

Reyes-Acosta, A.V., et al., 2019. 3D pipe reconstruction employing video information from mobile robots. Appl. Soft Comput. J. 75, 562–574. https://doi.org/10.1016/j.asoc.2018.11.016

Roh, S.G., Choi, H.R., 2005. Differential-drive in-pipe robot for moving inside urban gas pipelines. IEEE Trans. Robot. 21 (1), 1–17. https://doi.org/10.1109/TRO.2004.838000

Sergiyenko, O., et al., 2020. Sensors for structural health monitoring. Nanosensors for Smart Cities. Elsevier, pp. 227–248. https://doi.org/10.1016/B978-0-12-819870-4.00013-X

Shukla, A., Karki, H., 2016. Application of robotics in onshore oil and gas industry-a review Part i. Robot. Auton. Syst. 75, 490–507. https://doi.org/10.1016/j.robot.2015.09.012

Snavely, N., Seitz, S.M., Szeliski, R., 2006. Photo tourism. ACM SIGGRAPH 2006 Papers on - SIGGRAPH '06. ACM Pres,, New York, New York, USA, pp. 835. https://doi.org/10.1145/1179352.1141964

SPI Engineering (2020) 0.95mm Super-ultra Small Industrial Video Borescope HNL-0.95CAM120S. Available at: ⟨https://www.spieng.com/english/product/instant/hnl095cam_s.html⟩ (Accessed: 1 October 2020).

West, G., et al., 2015. Improved visual inspection of advanced gas-cooled reactor fuel channels. Int. J. Progn. Health Manag. 6 (SP3), 1–11.

Xie, R., et al., 2018. Automatic multi-image stitching for concrete bridge inspection by combining point and line features. Autom. Constr. 90, 265–280. https://doi.org/10.1016/j.autcon.2018.02.021

Zhang, D., et al., 2020. Quantifying impacts on remote photogrammetric inspection using unmanned aerial vehicles. Eng. Struct. 209, 109940. https://doi.org/10.1016/j.engstruct.2019.109940

Zhang, G., et al., 2016. Multi-viewpoint panorama construction with wide-baseline images'. IEEE Trans. Image Process. 25 (7), 3099–3111. https://doi.org/10.1109/TIP.2016.2535225

Zhang, X., et al., 2019. A 3D reconstruction pipeline of urban drainage pipes based on multiviewimage matching using low-cost panoramic video cameras'. Water (Switz.) 11 (10). https://doi.org/10.3390/w11102101